On the Mechanism of Formation and Growth of <100> Interstitial Loops in Ferritic Materials

Jaime Marian, Brian D. Wirth

Chemistry and Materials Science Directorate, Lawrence Livermore National Laboratory, P. O. Box 808, L-353, Livermore, CA 94550

and

R. Schäublin

CRPP, Fusion Technology-Materials, École Polytechnique Fédérale de Lausanne, CK-5232, Villigen PSI, Switzerland

Abstract

We propose a comprehensive mechanism for the formation and growth of <100> interstitial loops in α-Fe. This mechanism, which involves the formation of <100> junctions in the direct reaction between mobile <111> loops, reconciles long-standing experimental observations of these defects in irradiated ferritic materials with recent atomistic simulations of collision cascades and defect cluster properties in Fe, in which highly-mobile <111> clusters are seen to be the dominant feature. The <100> junctions, although metastable, grow into visible <100> loops as a consequence of the high kinetic barrier associated with rotation into <111> configurations and a very low mobility. Finally, the atomic character of 100 and $\frac{1}{2}\ 111$ loops is investigated with molecular dynamics simulations and the atomic configurations are used to calculate the defect image contrast through direct simulation of TEM images. The simulated images are subsequently compared with actual TEM micrographs of irradiated ferritic materials. Excellent agreement between the experiments and the simulations is found, allowing for a direct identification of the nature and structure of interstitial loops. Hence, this work provides one of the necessary links to unify simulation with experiments in α-Fe and ferritic alloys subject to high-energy particle irradiation.

Introduction

Ferritic steels and alloys represent a technologically important class of materials that are widely used for structural purposes in current nuclear fission reactors and proposed as candidate materials for plasma-facing first wall structures in future fusion energy facilities. Predicting their in-service performance requires understanding the accumulation of defects and evolution of the microstructure under the severe irradiation conditions found in these environments.

It is well established that examination of ferritic alloys by transmission electron microscopy (TEM) following low dose irradiation (<0.1 displacement per atom, dpa) by neutrons or heavy ions does not reveal any visible damage. However, as the irradiation dose increases above ~1 dpa, a significant population of prismatic dislocation loops, presumably of interstitial type, is experimentally observed. In contrast to other *bcc* alloys, such as Mo and V, the dislocation loops consist of Burgers vectors, b=<100> and b=<111>, in almost equal proportions, rather than predominantly <111> . While this result has been known for nearly 40 years [1-6] the mechanisms responsible for the presence of <100> loops in ferritic alloys are not yet well understood.

A comparison of the dislocation loop energy based on continuum elasticity estimates (elastic energy proportional to Gb^2, where G is the shear modulus), indicates that <111> loops are energetically favored and thus, the observation of <100> loops in α-Fe and other ferritic alloys has remained a puzzle. In 1965, Eyre and Bullough [7] proposed a mechanism by which <100>, as well as <111>, dislocation loops could form from an aggregate of <110> self-interstitials through shear reactions of the type:

$$\frac{1}{2}[110]+\frac{1}{2}[00\bar{1}] \rightarrow \frac{1}{2}[11\bar{1}]$$
$$\frac{1}{2}[110]+\frac{1}{2}[\bar{1}10] \rightarrow \frac{1}{2}[010] \qquad \text{(1 and 2)}$$

Again, consideration of the dislocation energy of the two reactions reveals a puzzle as to why <100> loops would form rather than <111>. Additionally, the Eyre and Bullough mechanism is predicated on the formation of platelets of self-interstitial atoms (SIA) with Burgers vector b=<110>, which corresponds to a faulted dislocation loop. However, the high stacking fault energy of *bcc* materials discounts the formation and stability of faulted loops and, thus, one can safely conclude that the Eyre and Bullough mechanism is not plausible to describe the formation of <100> interstitial loops in ferritic alloys.

Indeed, recent molecular dynamics (MD) simulations of self-interstitial cluster geometry using Finnis-Sinclair, embedded atom-type and long-range pair potentials reveal that stable interstitial cluster configurations for size from n>2 consist of aggregates of <111> -oriented, rather than <110>, split dumbbells [8-10]. Clusters of <111> self-interstitials have very high mobility for one-dimensional (1D) motion along <111> directions up to very large sizes (n>100). As well, MD simulations of displacement cascade evolution have consistently revealed the formation of SIA clusters with <111> orientations, which again exhibit high mobility [11,12]. Here we provide a mechanism for the formation and growth of <100> dislocation loops that reconciles the long-standing experimental observation of these defects in irradiated ferritic materials with recent MD studies of <111> cluster stability, their production in displacement cascades and high mobility in one dimension.

In this report, we first describe in detail the energetics of <111> and <100> interstitial dislocation loops, then propose a mechanism for <100>-loop nucleation, which involves the direct interaction of migrating <111> loops, and, finally, a growth mechanism for <100> loops to reach TEM visible sizes. An additional objective of this work is to investigate the correlation between dislocation loops produced by MD simulations and their observation in TEM by generating equivalent, conventional TEM (CTEM) images and assessing experimental limitations in the observation of small defect clusters. The weak beam technique [13] seems most appropriate in the case of small defects such as these, as it provides an improved spatial resolution and signal-to-background ratio over the usual bright/dark field mode of imaging in TEM, as well as a framework for direct comparison with actual experimental micrographs. Thus, by using a *virtual* electron microscope, this work tries to partially bridge the gap that exists between multiscale modeling and experiments within the study of radiation damage effects in metals.

Results

Loop energetics

Clearly, an energetics analysis based exclusively on isotropic, continuum elastic energy considerations (Gb^2) is insufficient to describe the loop interaction dynamics, as it ignores important contributions such as loop shape, angle between the habit plane and the Burgers vector,

and anisotropy effects. An analysis of the energetics of <111> and <100> loops that takes into account all such contributions is attained by way of fully-atomistic, MD relaxations at low temperatures, followed by a conjugate-gradient energy minimization to obtain the configuration-dependent loop energies. The configurations of interest for b=<100> loops are those with {110} and {100} habit planes (corresponding to the closest-packed and perfect edge configurations). In terms of loop shape, the minimum-energy configurations correspond to loop sides oriented along the close-packed directions in each habit plane, i.e. rhombic <100>{110} loops and square or rectangular <100>{100} loops (the most stable configuration for <111> loops has been reported to be hexagonal-shaped <111> {110} [9,10]. All atomistic results have been obtained with the MDCASK code [14] in which the Finnis-Sinclair-type potentials for Fe derived by Ackland et al. [15] have been implemented.

Figure 1 presents the three corresponding formation energy curves, obtained through a fit to the MD data (also shown) using the continuum elasticity expression for the self-energy, E_l, of a prismatic dislocation loop as given by Hirth and Lothe [16]:

$$E_l = \frac{NL\mu b^2}{4\pi(1-\nu)}\left(\ln\left(\frac{L}{\rho}\right) + C\right) \qquad (3)$$

Here N is the number of sides of the loop, L is the side length, μ and ν the shear modulus and Poisson's ratio, b is the Burger's vector magnitude and ρ and C represent the dislocation core cutoff radius and a constant that includes the dislocation core energy. Using the elastic constant values calculated from the α-Fe potential used here and values of ρ=b/4 and ρ=b for the cutoff radii of <111> and <100> loops, we obtain core energies of 0.38 and 1.10 eV/Å, respectively. The value for <111> loops is consistent with results reported in the literature [9,17] while, to our knowledge, the core energy value for the <100> dislocation loops represents the first calculation reported to date. The high value for both the dislocation loop core radii and core energy for <100> loops suggests the existence of large tensile forces around the core region of the loop, which diminishes the validity of a purely isotropic elastic analysis.

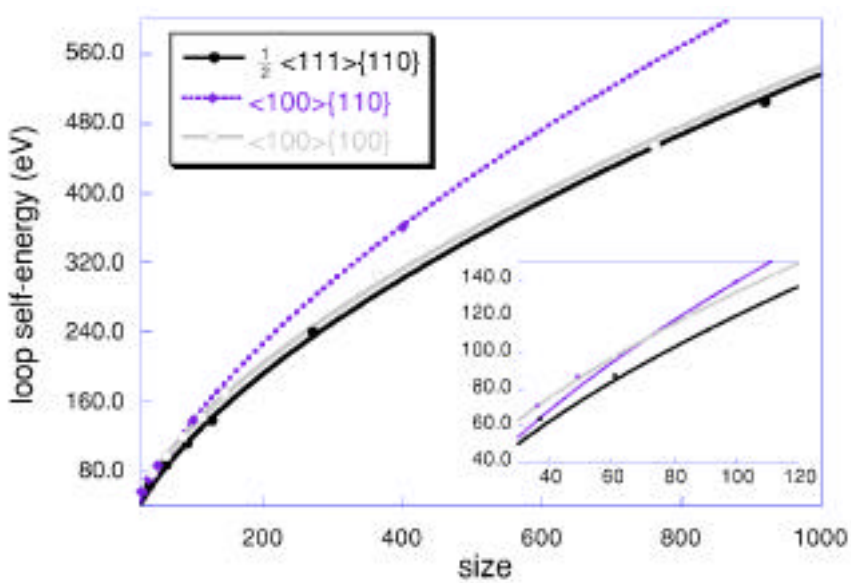

Figure 1:Dislocation loop energy as a function of size (number of constituent interstitials, n) for hexagonal <111>{110}, rhombic <100>{110} and square <100>{100} loops.

As seen in figure 1, <111> loops are the most stable configurations, consistent with previous continuum elasticity estimates, although the energy difference between <111> and <100>{100} configurations becomes very small (<10%) for larger loop sizes. Initially, <100> loops are more stable on {110} habit planes but, with increasing size, <100>{100} configurations become energetically favored, with a crossing around n~68. Presumably, this results from the reduction in dislocation segment length for <100> loops on {100} rather than {110} habit planes.

<u><100> loop formation</u>

It has long been recognized that reactions between dislocations with Burgers vectors b=<111> can occur according to:

$$\frac{1}{2}[111]+\frac{1}{2}[1\bar{1}\bar{1}]\rightarrow[100] \qquad (4)$$

This can lead to the formation of <100> junctions and dislocation segments, which have been mainly observed in dislocation networks in Fe [18,19]. As well, such reactions between <111>-type loops can give rise to the formation of <100> loops. Indeed, Masters proposed such a mechanism in 1965 [1], yet discounted it due to a lack of observed loops with b=<111> in thin-film ion irradiation studies.

In order to shed light onto the formation of <100> loops, we have performed extensive MD simulations of interactions between <111> loops. One such interaction consisted of hexagonal and jogged hexagonal <111> loops with n=37 and 34, respectively, with intersecting glide prisms, akin to equation 4. Figure 2 shows a sequence of snapshots from the MD simulation at 1000 K. The two loops glide towards one another and collide, driven by the energy reduction that results when two loops condense into a single loop containing the same total number of interstitials. A [100] junction consisting of five SIAs on a (110) plane formed instantaneously following the collision (figure 2b). Notably, Osetsky et al., using a long-range pair potential, observed a similar reaction between interstitial clusters in α-Fe. However, the <100> junction was unstable and dissolved after a short time at 800 K [20].

The peculiarity of this interaction is that the glide direction of each loop is contained in the habit plane of the other interacting loop, and thus, once the loops collide, the dislocation segments of Burgers vector [111] can continue to glide within the loop of Burgers vector $[\bar{1}\bar{1}1]$. By reaction (4), this produces dislocation segments with Burgers vector [100] on both sides of the contact point. Given enough time, both <111> loops will gradually transform into a single entity with Burgers vector b=<100>. Therefore, we propose that <100> loops initially form as <100> junctions on {110} planes in collisions between <111> loops and grow outward until the defect boundaries are reached. As the <100> segments grow and the elastic energy density (stress) builds up, the cluster will eventually rotate onto {100} habit planes. A large number of cluster-interaction simulations involving different cluster shapes and sizes have been performed, and, in all cases, the main observation is that the intersecting loops need to be of approximately the same size, and possibly shape, to stabilize and grow <100>-type segments. When these constraints are not met, the smaller cluster always rotates into the <111> orientation of the larger cluster.

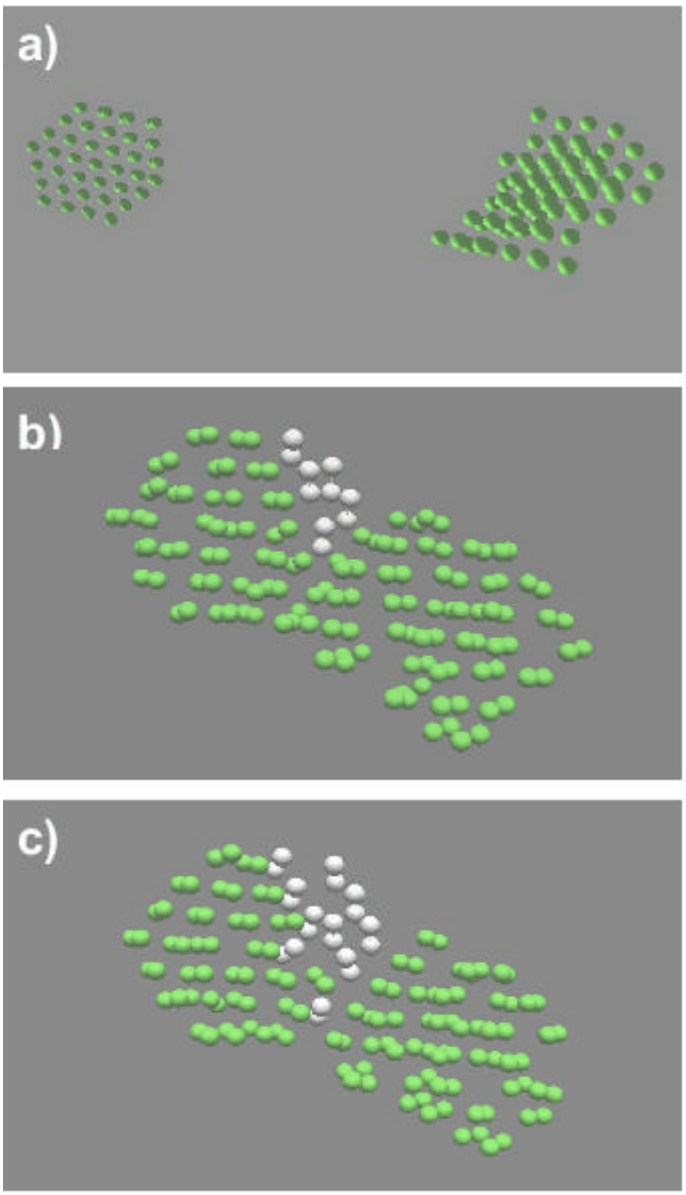

Figure2: Sequence of MD snapshots at (a) 0, (b) 120 and (c) 430 ps, of the interaction of two <111> loops with Burgers vectors appropiate to equation 4 at 1000 K. The loop on the left side of the image is a perfect, hexagonal 37-SIA cluster, while the one on the right is a 34-SIA jogged hexagonal loop. After forming a <100> junction following the loop collision, the junction expands throughout the resulting defect according to equations 5 and 6.

The high energies associated with having multiple dislocation segments within a loop make the propagation of the <100> segments a complex process at the atomic scale, since <111> dislocation segments no longer glide through perfect, close-packed directions but, instead, through a plane containing oppositely-oriented interstitials. Visualization of the MD simulations revealed that the <100> segments (best thought of as an array of akin self-interstitial atoms) propagate throughout the loop according to the following two-step reaction:

$$\frac{1}{2}[111]+\frac{1}{2}[00\bar{1}] \rightarrow \frac{1}{2}[110]$$
$$\frac{1}{2}[110]+\frac{1}{2}[1\bar{1}0] \rightarrow \frac{1}{2}[100] \qquad \text{(5 and 6)}$$

Thus, the interstitials reach their final [100] orientation by way of a modified Eyre-Bullough mechanism (modified reaction 1 and direct reaction 2). This is a thermally activated process by which SIAs at the <111>–<100> nodes, e.g with [111]-orientation, first undergo a partial $[00\bar{1}]$ shear into a metastable [110] configuration with an activation energy of ~0.5 eV. This produces large repulsive interactions with adjacent [100] dumbbells that force the metastable [110] dumbbell to further rotate into a more favorable configuration. This can be attained by the [110] dumbbell reversing its original trajectory back to the [111] orientation, or rotating into a [100] orientation through reaction 6, with an activation barrier of the order of 1.0 eV.

The nearly immediate formation of the <100> nucleus upon cluster collision is a consequence of the interaction process governed by equation 4 and driven by the energy reduction associated with forming a single cluster. The growth vs. shrinkage of the <100> junctions (loops) (equations 5 and 6) is governed by the interaction energy landscape, schematically shown in figure 3. The rate at which the growth of the [100] section is sampled (<111> to <110> to <100>) is favored with respect to its dissolution (inverse path), which, integrated over sufficiently long timescales, results in an effective <100>-loop transformation. For example, after 300 ps (figure 2(c)) five additional interstitials forming part of the $[1\bar{1}\bar{1}]$ loop rotated into a [100] orientation and resided in that configuration during the entire simulation (1 ns). The direct rotation from a <111> to a <100> orientation, or vice-versa, can be neglected, since it requires energies in excess of 2.0 eV. This provides an explanation as to why, at moderate temperatures, the final configuration resulting from the interaction of two <111> loops consists of metastable <100> loops, rather than the slightly lower-energy <111> loops.

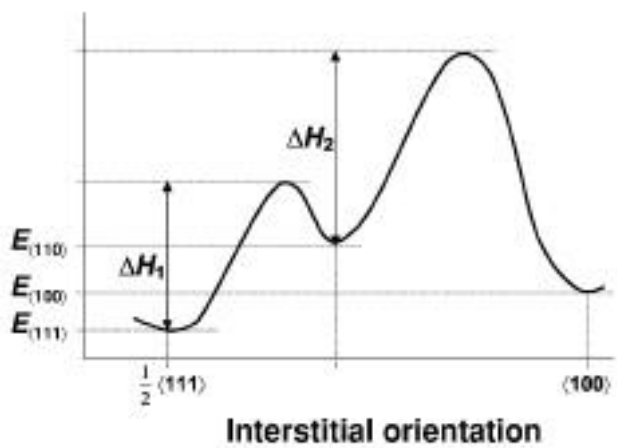

Figure 3: Schematic illustration of the energy landscape, projected along the reaction coordinate, for the propagation of <111> dislocation segments (best thought of as an array of individual SIAs) into <100> segments within the interacting <111> loops. The energy difference between each interstitial configuration is dependent upon loop size. ΔH_1 and ΔH_2 are of the order of 0.5 and 1.0 eV respectively.

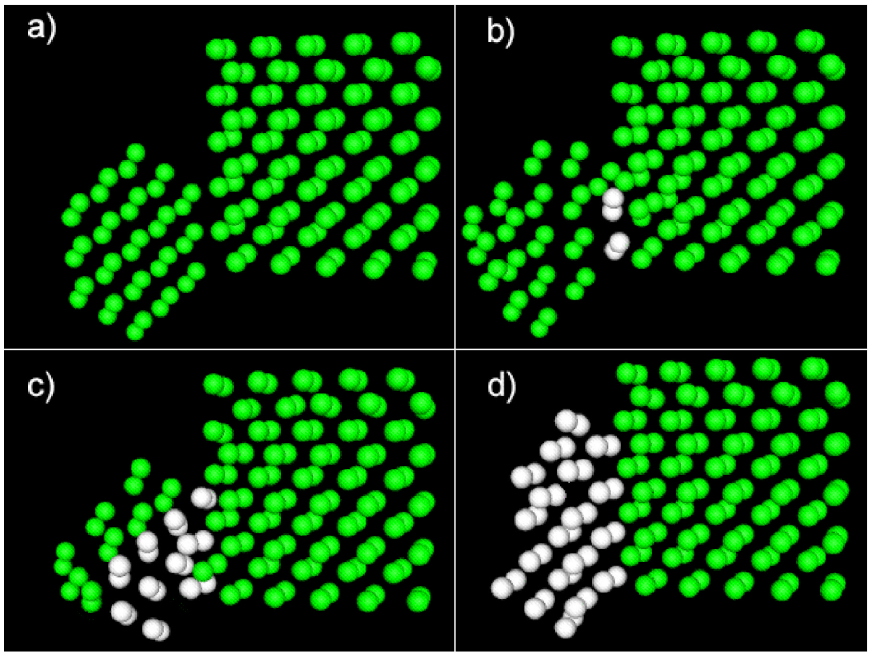

Figure 4: Sequence of MD snapshots at (a) 0.0, (b) 1.5, (c) 2.2 and (d) 3.5 ps, of the absorption of a hexagonal, 19-SIA [111](110) cluster by a square, 50-SIA [100](100) loop according to equation 7 at 100 K. Interstitials displayed in white are those belonging to the [111] cluster that have rotated to a [100] configuration.

<u><100> loop growth</u>

The remaining point to consider is how <100> clusters grow to TEM observable sizes. Although intrinsically glissile owing to their pure-edge prismatic nature, the bcc crystal structure dictates that <100>{100} loops require a large jump distance. This results in a very high activation energy, computed to be >2.5 eV. Thus, once formed, <100> loops are essentially stationary, and can become a sink for mobile, cascade-produced <111> loops. Notably, MD simulations of interactions between <111>{110} and <100>{100} loops reveal <100> loop growth. Figure 4 shows one such interaction in which a 19-SIA <111> cluster is absorbed by a 50-SIA <100> square loop. Even though the lowest energy configuration corresponds to a 69-SIA <111> loop, the system follows the path of least resistance into a 69-SIA <100> loop through the following atomic reaction:

$$\langle 100\rangle + 2\left(\frac{1}{2}\langle 111\rangle\right) \rightarrow \langle 211\rangle \rightarrow \langle 100\rangle \qquad (7)$$

i.e. rotation of individual <111>-oriented interstitials in the presence of <100> SIAs into an intermediate metastable <211> configuration that rapidly rotates into a <100> orientation.

<u>TEM image simulation, comparison with experiment</u>

The CTEM images of the dislocation loops are simulated using the multislice method [21] to obtain their weak beam image at 200 kV. This is performed with the EMS software package [22]. The most relevant parameter in this type of simulation is the objective aperture size. Ideally, for CTEM, and more precisely for weak-beam image simulation, the sample should be more than 10-nm thick to avoid surface effects, and thinner than 80 nm to reduce anomalous absorption, which arises from inelastic scattering of the electrons, that would result in a blurry image [23].

Details on the main elements of the approach are given elsewhere [24]. The sample obtained from MD simulations is cut perpendicular to the electron beam direction in slices 0.2-nm thick. The sample is in all cases cut into 100 slices that are roughly 10 nm on a side and contain approximately 2000 atoms. The diffraction condition is selected by the beam direction, parallel to the cutting direction, in order to isolate the systematic row defined by the chosen diffraction vector **g**. In this work the diffraction vector was picked to be **g**=(200) and the diffraction condition was **g**(4.1**g**). The parameters used to obtain the images are similar to those of modern microscopes operated at an acceleration voltage of 200 kV.

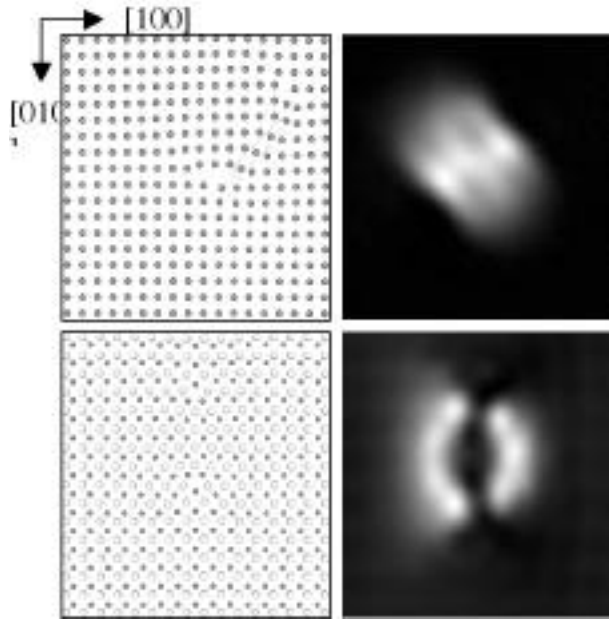

Figure 5: [001] view of the MD simulation box after relaxation of a $\frac{1}{2}[111]$ (top image) and a [100] (bottom) loop respectively. Next to each one of the atomistic images are the corresponding weak beam, **g**=(200), **g**(4.1**g**), CTEM simulated images.

Figure 5 shows the CTEM simulated images of a 91-SIA, hexagonal, $\frac{1}{2}$ 111 {110} loop and a 61-SIA, hexagonal, 100 {100} loop, taken under the above conditions. A cut perpendicular to the [001] direction of the simulation box for each loop is also shown. The observed contrast in the images originates from the defect-induced displacement field. From the images, it is clear that the displacement field caused by the $\frac{1}{2}$ 111 loop is mostly circumscribed to the glide prism of the defect, while on the contrary, for the 100 loop, the strain field has stereoscopic geometry and reaches outside the glide prism of the loop. This is likely a consequence of the larger dislocation core volume for 100 interstitial loops, whereas the compressive stress caused by $\frac{1}{2}$ 111 loops is more easily accommodated along close-packed 111 directions, with even small tensile regions appearing in between the main twin compressive lobes of the individual crowdions that constitute the cluster [25]. This means that the displacement field induced by the loops in the direction perpendicular to the Burgers vector is virtually non-existent, although this is not so clearly appreciated in the image of the $\frac{1}{2}$ 111 loop, since the diffraction vector is not parallel to the Burgers vector (**b**×**g**≠0). Another interesting feature is that while the 100 loop clearly lies on two

consecutive *AB* (200) planes (to conserve the stacking sequence *ABAB*), the $\frac{1}{2}\ 111$ rests on several $(1\bar{1}\ 0)$ planes through kinks that are weakly distinguishable in the image. The double *bean* contrast observed in the 100 image is characteristic of interstitial dislocation loops in metals, irrespective of their Burgers vector. This includes $\frac{1}{2}\ 111$ clusters in Fe, as recognized in several experiments where $\frac{1}{2}\ 111$ loops were observed edge-on (**b**×**g**=0) [26].

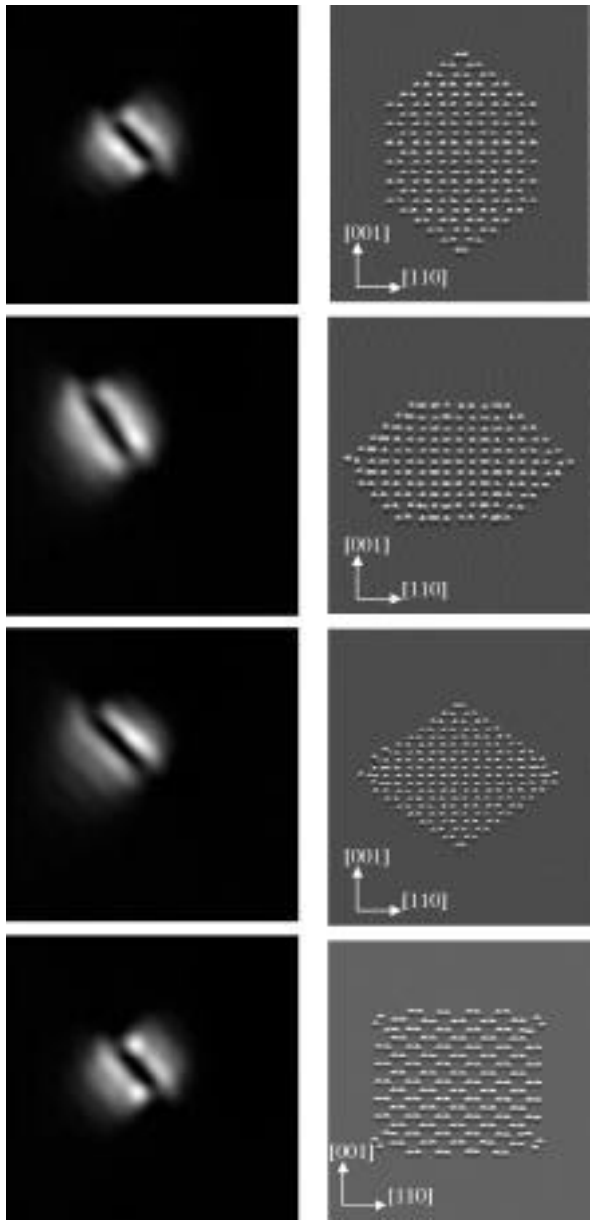

Figure 6: CTEM simulated images (left) of $100\ \{110\}$ loops with different sizes and shapes (right). The atomic configurations on the right are viewed from a $[1\ \bar{1}0]$ direction.

The shape of the dislocation loops does not seem to have a significant effect on the simulated images, although it significantly influences the loop self-energies. Figure 6 shows a series of 100 {110} loops of different sizes and their associated weak-beam images, which indicates that little information about the shape of the loops can be extracted using this set of CTEM imaging conditions. The images are qualitatively similar to that of the previous 100 {100} loop of figure 5, with the double-bean contrast clearly observed in all cases.

The results for loop energetics shown in figure 1 agree well with experiments [27,28] in that, for sizes larger than 65~70 SIAs, 100 loops are most stable on {100} planes. For the purpose of directly comparing the simulated images with actual TEM micrographs, an irradiated tempered martensite steel sample was analyzed in the microscope. Figure 7 shows an experimental TEM, weak beam, **g**(4.1**g**), **g**=(200) image of a F82H (Fe-9Cr) tempered martensite steel sample. The material was neutron irradiated at high dose rate and 302˚C, up to a total dose of 8.8 dpa in the HFR facility in Petten. The observed microstructure contains a number of features, most of which are defect clusters generated by the irradiation. The two insets displayed in figure 7 represent an 18-nm long, 937-SIA, rectangular, 100 {100} loop (A–bottom right) and a 4-nm, 91-SIA, hexagonal, 100 {100} loop (B–top left). Both loops exhibit characteristics that can be qualitatively recognized in the experimental micrograph, where two defects with similar size and contrast have been pointed out (A and B). These are interstitial dislocation loops with 100 Burgers vector and lying on {100} planes. We emphasize the excellent agreement between the simulations and the experimental observations.

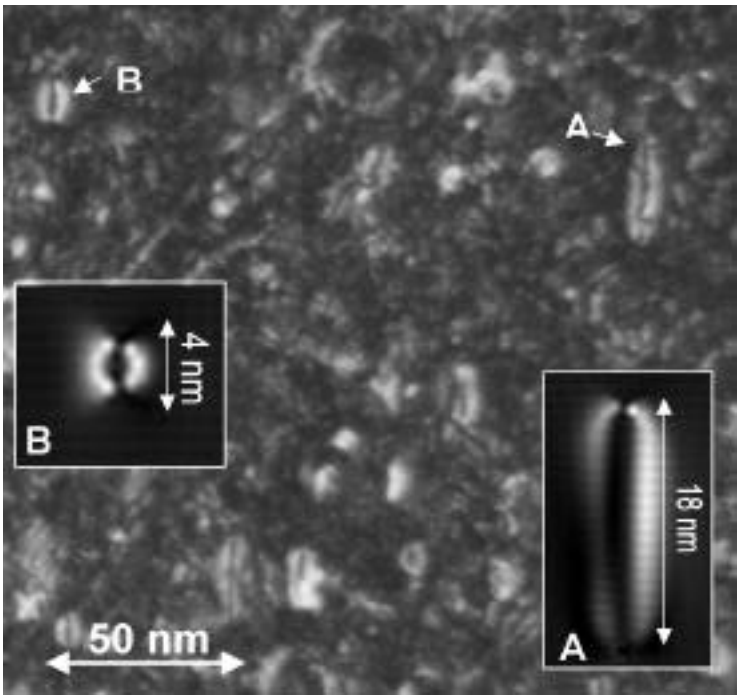

Figure 7: Experimental TEM weak beam image of a Fe-9Cr crystal irradiated with neutrons to a dose of 8.8 dpa at 302˚C. The two insets represent CTEM simulated images of (A) an 18-nm, rectangular [100] loop and (B) a 4-nm, hexagonal, [100] loop. A number of features can be observed in the TEM micrograph, among which two (A and B) interstitial loops with Burgers vector [100], sitting on {100} planes, can be identified. The agreement with the simulated loops in both contrast and shape is excellent.

Summary

In summary, based on extensive MD simulations of <111>–<111> and <100>–<111> interactions, we propose a comprehensive mechanism for the nucleation and growth of TEM visible <100> loops. This mechanism is consistent with both experimental observations and with the current understanding of interstitial cluster formation, diffusion and growth from atomistic simulations.SIAs produced in collision cascades initially aggregate as small <111> clusters. These clusters either rapidly migrate to system sinks or interact with each other. <100> nuclei form through the direct interaction of <111> clusters of comparable size via equation 4. The two interacting dislocation loops propagate through each other's habit plane according to reactions 5 and 6, resulting in the ultimate growth of the <100>{110} junction until the whole loop is transformed. The resulting loops are metastable with respect to <111>, but the energy differences can be quite small and the activation barrier to re-orient into <111> orientations quite large. With increasing size, n>68, <100>{110} loops re-arrange onto {100} habit planes. In this configuration, <100> loops are metastable and practically immobile, allowing for the absorption of other small <111> clusters via a direct-rotation mechanism (reaction 7) that allows <100>-loop growth up to TEM observable sizes.

Weak beam, CTEM images for a number of loops of different Burgers vectors, habit planes, sizes and shapes using **g**=(200) and **g**(4.1**g**) have been generated. Useful information about the induced strain field can be extracted from the CTEM simulated images in each case. The observed strain field of $\frac{1}{2}$ 111 loops remains mostly confined to the loop glide prism whereas that of 100 clusters extends beyond the limits of the prism, with the CTEM image conditions chosen. Loop shape does not have any significant impact on the simulated images, which all exhibit the well known, double-bean contrast of SIA loops.

Finally, qualitative agreement between the simulated images and actual experimental micrographs taken from one specific experiment of a Fe-9Cr sample is found to be excellent, which validates the use of this technique to identify the nature of interstitial clusters in irradiated ferritic materials.

The authors acknowledge many helpful discussions with Drs. W. Cai and V. Bulatov and are grateful to J. W. Rensman of the HFR facility at Petten, for providing the Fe-9Cr specimen for the TEM analysis. This work has been performed under the auspices of the U.S. Department of Energy and Lawrence Livermore National Laboratory under contract W-7405-Eng-48 and within the CSN-UNESA Coordinated Research Programme under contract P000531499.

References

[1] B. C. Masters, *Phil. Mag*. **11**, 881 (1965)
[2] B. L. Eyre and A. F. Bartlett, *Phil. Mag*. **11**, 261 (1965)
[3] B. L. Eyre and A. F. Bartlett, *J. Nucl. Mater*. **47**, 143 (1973)
[4] T. J. Bullough and B. L. Eyre, *Proc. R. Soc. Lond. A* **435**, 85 (1991)
[5] H. Kawanishi and E. Kuramoto, *J. Nucl. Mater*. **141-143**, 899 (1986)
[6] L. L. Horton and K. Farrell, *J. Nucl. Mater*. **122-123**, 687 (1983)
[7] B. L. Eyre and R. Bullough, *Phil. Mag*. **12**, 31 (1965)
[8] R. A. Johnson, *Phys. Rev*. **134**, 1329 (1964)
[9] B. D. Wirth, G. R. Odette, D. Maroudas and G. E. Lucas, *J. Nucl. Mater*. **276**, 33 (2000)
[10] Y. N. Osetsky, A. Serra, B. N. Singh and S. I. Gobulov, *Phil. Mag*. *A* **80**, 2131 (2000)
[11] R. E. Stoller, *J. Nucl. Mater*. **237**, 299 (1996)

[12] N. Soneda and T. Díaz de la Rubia, *Phil. Mag. A* **78**, 995 (1998)
[13] D. J. H. Cockayne, I. L. F. Ray and M. J. Whelan, *Phil. Mag.* A **20** (1969) 1265
[14] T. Díaz de la Rubia and M. W. Guinan, *Mater. Res. Forum* **174**, 151 (1990)
[15] G. J. Ackland, D. J. Bacon, A. F. Calder and T. Harry, *Phil. Mag. A* **75**, 713 (1997)
[16] J. P. Hirth and J. Lothe, *Theory of Dislocations, 2nd ed.* (Krieger Publishing Co., Malabar, FL, 1982)
[17] J. O. Schiffgens and K. E. Garrison, *J. Appl. Phys.* **43**, 3240 (1972)
[18] W. Carrington, K. F. Hale and D. McLean, *Proc. R. Soc. Lond. A* **259**, 203 (1960)
[19] S. M. Ohr and D. N. Beshers, *Phil. Mag.* **8**, 1343 (1963)
[20] Y. N. Osetsky, A. Serra and V. Priego, *J. Nucl. Mater*. **276**, 202 (2000)
[21] J. M. Cowley and A. F. Moodie, *Acta Crystallographica* **10** (1957) 609
[22] P. A. Stadelmann, *Ultramicroscopy* **21** (1987) 131
[23] W. M. Stobbs and C. H. Sworn, *Phil. Mag.* **24** (1971) 1365
[24] R. Schäublin, A. Almazouzi, Y. Dai, Y. N. Osetsky and M. Victoria, *J. Nucl. Mat* **276** (2000) 251
[25] J. Marian, B. D. Wirth, J. M. Perlado, G. R. Odette and T. Díaz de la Rubia, *Phys. Rev.* B **64**, 094303 (2001)
[26] A. E. Ward and S. B. Fisher, *J. Nucl. Mat* **166** (1989) 227
[27] D. S. Gelles, M. L. Hamilton and R. Schäublin, in *Effects of Radiation on Materials: 20th International Symposium, ASTM STP 1405*, S. T. Rosinski, M. L. Grossbeck, T. R. Allen and A. S. Kumar, Eds., American Society for Testing and Materials, West Conshohocken, PA, 2002
[28] E. A. Little, R. Bullough and M. H. Wood, *Proc. Royal. Soc. London* A **372** (1980) 565